

# Design of a SWIPT System With Special Consideration of the Near-Field WPT in the 27 MHz Band

*Ghulam Murtaza, Mazen Shanawani, Diego Masotti, and Alessandra Costanzo*

*Abstract* – This article takes into account the simultaneous wireless information and power transfer (SWIPT) application in a railway scenario, with special consideration of the near-field wireless power transfer (WPT) system and its coexistence with neighboring subsystems. Therefore, many solutions, as well as geometrical aspects, are considered to virtually isolate the WPT system from the rest of the system without losing the requisite criteria for the WPT. As a peculiarity of the work, the system is considered as a whole, from the biasing of the inverter on the transmitting side to the receiving loop load. Furthermore, the study also highlights aspects of near-field SWIPT to a moving receiver that makes the problem at hand more complex.

## 1. Introduction

Simultaneous wireless information and power transfer (SWIPT) is a technique receiving more and more attention from the scientific community with each passing day. Initially, the idea of SWIPT was proposed for the receiver having ability to receive power and information from the same signal simultaneously [1], even if it was not realizable for the practical reasons highlighted in [2]. However, various techniques were evolved over the years to make SWIPT possible through power-splitting and time-switching methods [3, 4]. The authors in [5] used the concept of SWIPT by sending power on the fundamental harmonic and sending information on the higher harmonics. Similarly, multifrequency SWIPT was discussed in [6]. The two frequency near-field SWIPTs discussed in [5] makes use of the same resonant receiving section for power and communication. Near- and far-field SWIPT applications are presented in [7, 8], but they take into consideration a capacitively coupled resonant link that is more sensitive to the surroundings [9]. However, the near-field SWIPT in multifrequency and moving receiver

applications is not widely reported in the literature. In SWIPT applications, the wireless power transfer (WPT) systems are integrated with other subsystems that need to be electrically isolated from the power transmitter, and for the near-field WPT, the situation becomes more complex. The presence of neighboring subsystems can alter the field distribution between the power transmitter and the receiver, significantly. This article, starting from the preliminary results shown in [10], proposes a solution to reduce the unwanted coupling between colocated subsystems with powering, communication, and test functions. Different from the literature, it manages the entire system, including the wireless link, the nonlinear transmitting amplifier, and the receiving coil as a whole. Besides the full-wave description of the resonant link, this article focuses on the strategic role played by the choice of the power amplifier on the global efficiency and the methodology adopted to improve it.

To keep the study in line with the existing railway systems, the choice of the coil operating frequencies at 27.095 MHz and 4.234 MHz for the powering and communication operations, respectively, has been done according to the European Rail Traffic Management System [11]. The role of the test coil is more of an auxiliary nature, imposed by the high safety integrity level requested in railway systems. The operating frequency of this coil has been fixed at 6 MHz and is, therefore, close enough to the communication frequency: it has to periodically verify the functionality of the communication link through a loosely coupled operating condition. Although the communication link is well standardized within the railway framework, so little change in the system is envisaged, there is still space for significant improvements in the power side of the SWIPT architecture: this article aims to bridge this gap.

## 2. Description of the Problem

We can consider two separate goals in our design. The first one relies on the optimization of the power transmitter by taking into account a moving receiver that changes its position with respect to the transmitter. The electrical isolation of the transmitter from the other subsystems for SWIPT purposes is also addressed.

Figure 1 shows the scheme of the planar coils on the power transmitting side of the link, where the red spots indicate the feeding port placement. There are three different coils working at various frequencies. The

Manuscript received 29 August 2020.

Ghulam Murtaza is with DEI Department of Electrical, Electronic, and Information Engineering “Guglielmo Marconi”, University of Bologna, Viale Risorgimento 2, Bologna, Italy; e-mail: ghulam.murtaza2@unibo.it.

Mazen Shanawani, Diego Masotti, and Alessandra Costanzo are with DEI-ARCES Department of Electrical, Electronic, and Information Engineering “Guglielmo Marconi”, University of Bologna, Viale Risorgimento 2, Bologna, Italy; e-mail: mazen.shanawani@unibo.it, diego.masotti@unibo.it, alessandra.costanzo@unibo.it.

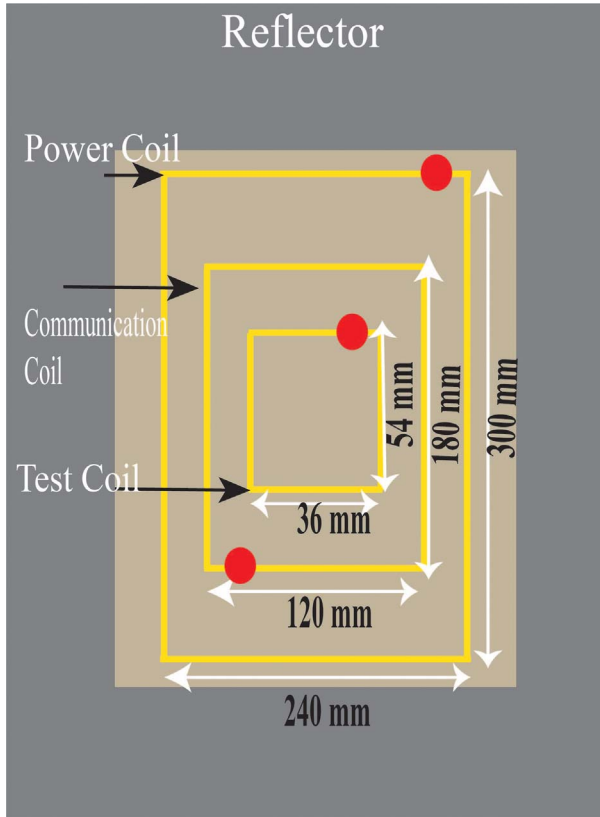


Figure 1. Multiple coil layout at the transmitter side.

outermost coil represents the power transmitting one working at 27.095 MHz, sending the power to wake up the inductively coupled receiving coil. It has inductance of 896 nH, with a lumped series resonant capacitor of 38.5 pF. The inner two coils represent two colocated and independent subsystems working at 4.234 MHz and at 6 MHz, respectively. The first one is the communication coil responsible for the reception of telegrams from the woken coil on the other side of the link and provides 398 nH of inductance, with 3.5 nF as the lumped series resonant capacitor. The smallest coil is placed for test purposes and is not needed for high efficiencies. For all three coils, the thickness of the copper layer is 70  $\mu\text{m}$ , and its width is 7 mm. As mentioned previously, the receiver is not static; therefore, vertical movements away from the transmitter with displacements in the range of 200 mm to 400 mm are considered. As can be evinced from Figure 1, an aluminum reflector is placed behind the coils at a distance of 80 mm to decouple the SWIPT system from the background.

Keeping in mind the nonlinearity involved in the design of the inverter, a wideband full-wave electromagnetic description of the wireless link is done to ensure that the overall design is very close to the actual situation. For this purpose, a similar multicoil receiving system is considered.

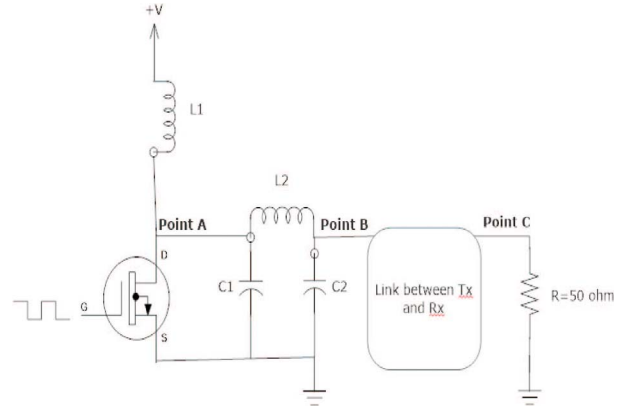


Figure 2. Schematic of the adopted class-E inverter.

### 3. Design of the Amplifier for the Moving Receiver

In Figure 2, the circuit schematic for the WPT subsystem is shown. The figure shows a class-E inverter topology. Class-E inverters are designed for specific loads; however, in this case, the loading conditions are not a priori known. Consequently, a  $\pi$ -matching network is placed between the inverter and the wireless link. This network plays a strategic role in the optimization of the system for different loading conditions.

A harmonic balance (HB) optimization has been carried out, asking for maximum inverter efficiency and power at the power coil input port (point B of Figure 2) around 30 W. This last goal derives from preliminary calculations performed in the higher separation case (400 mm): because of the poor coupling, the adopted power level guarantees more than 60 mW in the receiver side, considered as a minimum wake-up threshold. The result of the optimization in terms of components values are  $L1 = 80 \mu\text{H}$ ,  $L2 = 23.5 \text{ nH}$ ,  $C1 = 228 \text{ pF}$ , and  $C2 = 5 \text{ pF}$ . A 50% duty cycle with a 27.095 MHz pulse is used to drive the gate terminal of the GaN high electron mobility transistor GaN HEMT (GaN Systems (U.S.A.) GS66508b). The amplifier circuit is fed with a 9 V dc source, which is also an output from the optimization procedure and can be easily obtained onboard.

Both the choices of a switching inverter topology and a GaN transistor as the switching device lead to a high-efficiency solution. The *soft-switching* technique is also adopted to minimize the switching losses, hence, to enhance the efficiency of the class-E inverter. It consists of two basic conditions on the output voltage of the class-E inverter to be guaranteed while optimizing: 1) the voltage should be zero at  $\omega t = 2\pi$ , zero voltage switching (ZVS); and 2) first derivative of the voltage should also be zero at  $\omega t = 2\pi$  (zero derivative switching).

Compared with time domain transient analysis, the HB technique can provide a deep inside into the steady state behavior of the nonlinear circuit over the

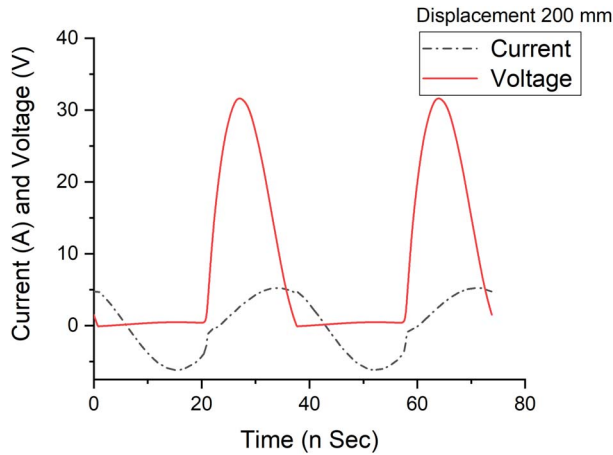


Figure 3. Voltage and current waveforms at point A.

simulated harmonics. By knowing and controlling the frequency response of the circuit linear part, the HB technique allows manipulation of the steady state values of harmonic components of current and voltages, an added advantage for the designer to tailor different harmonics according to the requirement. For the accurate description of the problem, 80 harmonic components are used to describe the gate pulse. As a consequence, an equally wideband full-wave electromagnetic representation of the wireless link is also provided.

#### 4. Numerical Results for Varying Link distances

By referring to the sections highlighted in Figure 2 and considering real components (including parasitics), we can see in Figures 3 and 4 that the voltage at point A has a good ZVS condition for the two distances of 200 mm and 400 mm between transmitter and receiver, respectively. Note that besides the reduction of losses, ZVS is important because, if not satisfied, the amplifier

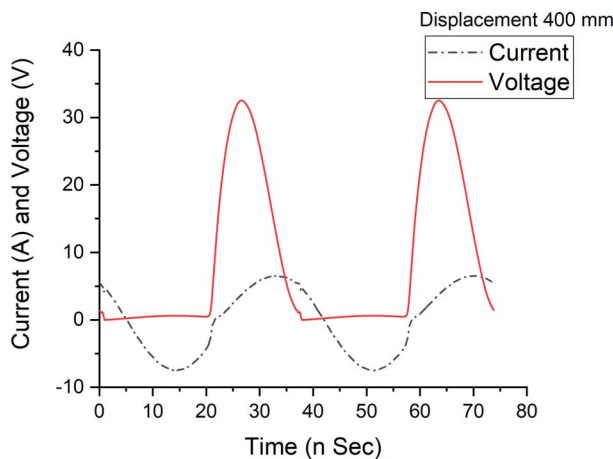


Figure 4. Voltage and current waveforms at point A.

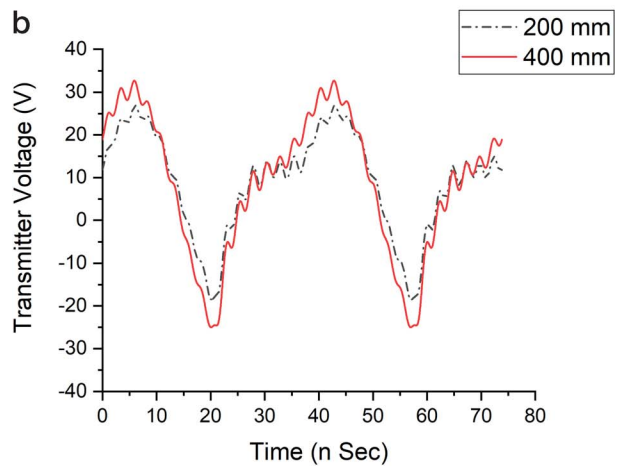
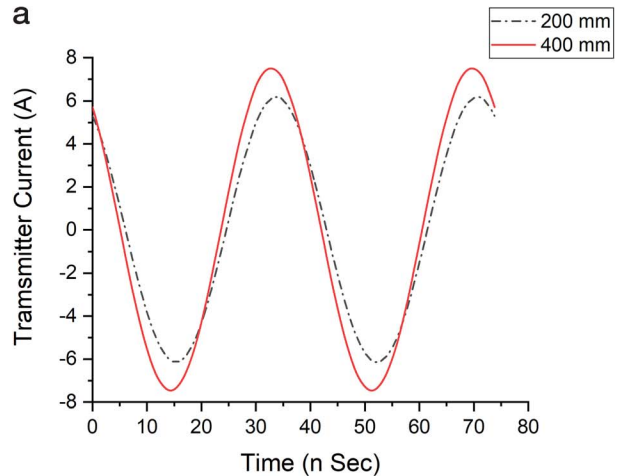


Figure 5. (a) Current and (b) voltage waveforms at point B for two link distances.

biasing condition (hence, the input power level) increases: this can damage the GaN device and also drastically reduce the efficiency.

By observing the current waveforms, note that the current is not zero in correspondence of the ON period of the voltage, which leads to some losses. This is a consequence of the real GaN switch model. For an ideal switch, these losses can be avoided [10], and the inverter efficiency is better than 90%. Moreover, despite the significant change of the link distance, the waveforms of Figures 3 and 4 are almost identical, as a demonstration of the class-E inverter independency on the loading conditions.

Voltage and current waveforms at point B are shown in Figure 5. The voltage waveform in Figure 5b shows the presence of higher harmonics generated by the highly nonlinear behavior of the GaN switch. This harmonic content is filtered out by the introduction of the resonant capacitor in series with the power coil (as demonstrated by the corresponding sinusoidal waveforms of Figure 6).

As per the design goals, power levels at the power coil port (point B) are 30 W and 22 W for distances of

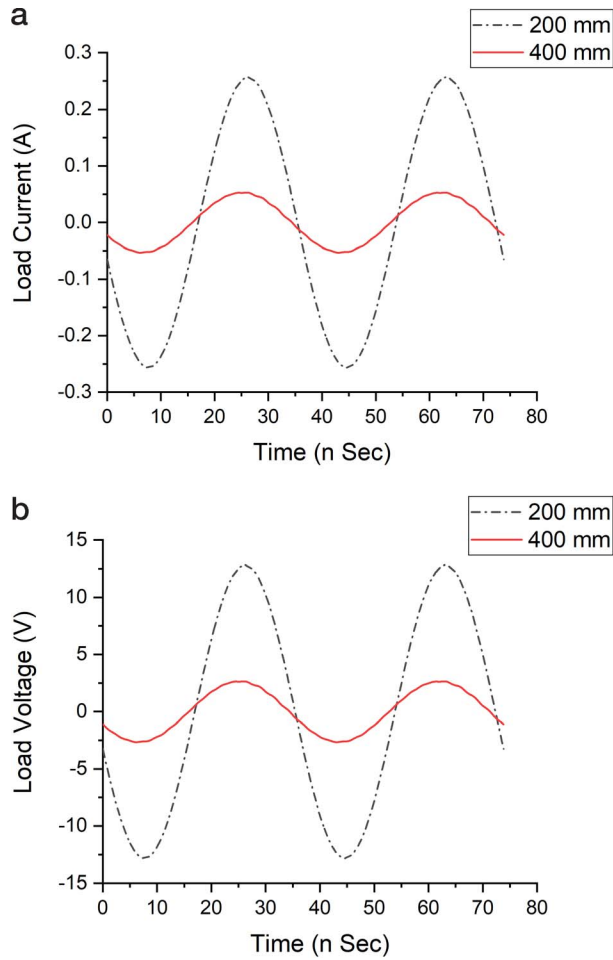


Figure 6. (a) Current and (b) voltage waveforms at point C for two link distances.

400 mm and 200 mm, respectively. Efficiency of the inverter in both cases is around 75%, again assuring the load-independent behavior.

With the increase in distance, the coupling factor [10] between transmitter and receiver, of course, reduces; hence, lower power levels are retrieved at the load end. Figure 6 shows the pure sinusoidal voltage and current waveforms obtained at the load end (hence, after the wireless link), indicated as point C in Figure 2.

Power delivered to the  $50 \Omega$  load is 1.6 W and 0.07 W for distances of 200 mm and 400 mm, respectively. Efficiency of the entire link varies between 7% to 0.2% for the movement of the receiver between the two distances. All the results of this section are obtained with the optimum topology, including the trapping filters, described in the following section.

## 5. Isolation of the Power Subsystem From the Colocated Subsystems

The presence of the many subsystems gives rise to unwanted coupling among them. Without any precautions, most of the power at 27.095 MHz is coupled to

Table 1. Coupled power for communication and test coils with different spacing

| Link distance       | 200 mm              |           | 400 mm             |           |
|---------------------|---------------------|-----------|--------------------|-----------|
|                     | Communication coil* | Test coil | Communication coil | Test coil |
| Without filters (W) | 19                  | 0.07      | 18.6               | 0.07      |
| With filters (W)    | 0.7                 | 0.002     | 1                  | 0.003     |

the communication and test coils; in particular, with the communication coil because of its proximity with the power coil (see Figure 1). A strategic electromagnetic decoupling of the communication and the test coils from the power coil can be obtained through the placement of two trapping filters. The trapping filter is thought of as a retrofitted system to protect the flow of high power levels at 27.095 MHz in highly coupled systems. As the communication is narrow band, the trapping filter is designed so that it gives a very minimum series impedance at the frequency of interest 4.234 MHz or 6 MHz ( $\sim 200$  mW) and acts as a high ( $\sim 1.5$  kW) series impedance to block the power at 27.095 MHz.

Although in a retrofitted setting as the one suggested here, a study of the impact the trapping filter has on the signal-to-noise ratio would be necessary. It is expected that the trapping filter will have little or a positive impact, as the communication band is very narrow, and the trapping filter helps block the unwanted wideband noise signals.

Table 1 shows the power coupled to the communication and test coil, with and without the trapping filters (leaving unchanged the other component values, as given in the previous paragraphs). We can see considerable improvement due to the presence of the trapping filters.

## 6. Conclusion

This work undertakes a practical scenario for a SWIPT application in which many subsystems are working at different frequencies. Special consideration is given to the inductive WPT system. Furthermore, the design of the GaN-based class-E power amplifier has been adopted to ensure a constant current source despite the mobile receiver. In addition to this, a trapping filter mechanism is introduced to electrically isolate the subsystems, so unwanted power coupling can be reduced significantly. The HB-based optimization of the multifrequency system is carried out by considering the entire chain of the subsystems as a whole, simultaneously taking control of the different dynamic phenomena characterizing the strongly nonlinear regime of the system.

## 7. References

1. P. Grover and A. Sahai, "Shannon Meets Tesla: Wireless Information and Power Transfer," IEEE International Symposium on Information Theory, Austin, TX, USA, June 13–18, 2010, pp. 2363–2367.
2. I. Krikidis, S. Timotheou, S. Nikolaou, G. Zheng, D. W.

- K. Ng, et al., "Simultaneous Wireless Information and Power Transfer in Modern Communication Systems," *IEEE Communications Magazine*, **52**, 11, November 2014, pp. 104-110, doi: 10.1109/MCOM.2014.6957150.
3. Q. Shi, C. Peng, W. Xu, M. Hong, and Y. Cai, "Energy Efficiency Optimization for Miso SWIPT Systems With Zero-Forcing Beamforming," *IEEE Transactions on Signal Processing*, **64**, 4, February 2016, pp. 842-854.
  4. H. Ju and R. Zhang, "Throughput Maximization in Wireless Powered Communication Networks," *IEEE Transactions on Wireless Communications*, **13**, 1, January 2014, pp. 418-428, doi: 10.1109/TWC.2013.112513.130760.
  5. J. Wu, H. Zhang, P. Gao, Z. Dou, N. Jin, et al., "Dual-Frequency Programmed Harmonics Modulation-Based Simultaneous Wireless Information and Power Transfer System via a Common Resonance Link," *Sustainability*, **12**, 10, May 2020, pp. 1-14, doi: 10.3390/su12104189.
  6. W. Liu, K. T. Chau, C. H. T. Lee, C. Jiang, W. Han, et al., "Multi-Frequency Multi-Power One-to-Many Wireless Power Transfer System," *IEEE Transactions on Magnetics*, **55**, 7, July 2019, pp. 1-9, doi: 10.1109/TMAG.2019.2896468.
  7. M. Del Prete, F. Berra, A. Costanzo, and D. Masotti, "Seamless Exploitation of Cell-phone Antennas for Near-Field WPT by a Frequency-Diplexing Approach," *IET Microwaves Antennas & Propagation*, **11**, 5, April 2017, pp. 649-656, doi: 10.1049/iet-map.2016.0281.
  8. R. Trevisan and A. Costanzo, "A UHF Near-Field Link for Passive Sensing in Industrial Wireless Power Transfer Systems," *IEEE Transactions on Microwave Theory and Techniques*, **64**, 5, May 2016, pp. 1634-1643, doi: 10.1109/TMTT.2016.2544317.
  9. G. Monti, M. Mongiardo, F. Matri, A. Costanzo, L. Corchia, et al., "Non-Radiative Wireless Power Transmission: Theory and Applications," in S. Nikolettas Y. Yang, A. Georgiadis (eds.), *Wireless Power Transfer Algorithms, Technologies and Applications in Ad Hoc Communication Networks*, Cham, Switzerland, Springer, 2016, Chapter 1.
  10. G. Murtaza, M. Shanawani, D. Masotti, and A. Costanzo, "Optimization of a 27 MHz Wireless Power Transmitter for Unknown Receiver," Thirty-Third General Assembly and Scientific Symposium of the International Union of Radio Science, Rome, Italy, October 20, 2020, doi:10.23919/URSIGASS49373.2020.9232315.
  11. European Rail Traffic Management System, "ERTMS/ETCS System Requirements Specification/SUBSET-036," [https://www.era.europa.eu/content/set-specifications-3-etcs-b3-r2-gsm-r-b1\\_en](https://www.era.europa.eu/content/set-specifications-3-etcs-b3-r2-gsm-r-b1_en). (Accessed 28 August 2020).